

# Improving the thermal stability and phase change speed in $\text{Sb}_{70}\text{Se}_{30}$ films through Er doping

Hua Zou<sup>1</sup> · Xiaoqin Zhu<sup>1</sup> · Yifeng Hu<sup>1</sup> · Yongxing Sui<sup>1</sup> · Jianhao Zhang<sup>1</sup> · Zhitang Song<sup>2</sup>

Received: 19 June 2017 / Accepted: 12 August 2017 / Published online: 20 August 2017  
© Springer Science+Business Media, LLC 2017

**Abstract** For the phase change memory (PCM) application, it is very desirable to possess better comprehensive performance in phase change materials, such as high stability, ultra-faster phase change and low power consumption. In this work, Er doped  $\text{Sb}_{70}\text{Se}_{30}$  phase change materials were synthesized by magnetron sputtering technique. Compared with pure  $\text{Sb}_{70}\text{Se}_{30}$  films, it was found that the crystallization temperature ( $T_c$ ) increased from 207 to 221 °C by Er doping, revealing the improvement of thermal stability. In addition, the increasing resistance of amorphous and crystalline state indicated much lower power consumption for PCM. More importantly, the Er doping significantly inhibits the formation of Sb–Se phase, which is to result in much faster phase change speed. Therefore, this work elucidated that the SbSe materials with Er doping were promising candidates possessing better data retention, lower power consumption and faster phase change speed for PCM application.

## 1 Introduction

In the new era, it is becoming increasingly important to develop next generation nonvolatile memory due to the

immense increasing of data memory requirement [1]. Phase change memory (PCM) is one of the most promising candidates possessing many advantages, such as long cycle life, low programming energy, and excellent scaling characteristics, etc. [2, 3]. The data storage capability of PCM is achieved from the resistance differences between amorphous (RESER state-logic “0”) and crystalline (SET state-logic “1”) [4, 5]. Among various phase change materials,  $\text{Ge}_2\text{Sb}_2\text{Te}_5$  (GST) has been widely adopted due to their exceptional characteristics such as high resistance contrast, ultrafast switching speed and best scalability [6]. However, there is no material system that can possess good performance in all respects [7, 8].

Compared with GST, SbSe phase change alloys have a lower melting temperature and high phase change speed [9]. In addition, their sheet resistance differences between the amorphous and crystalline state are higher than  $10^4 \Omega$ . Sung-Min et al. have demonstrated that the SbSe based PCM device have lower power and much higher speed compared with GST based memory [9]. Kang et al. have investigated the phase change properties of  $\text{Sb}_x\text{Se}_{100-x}$ , indicating the activation energy ( $E_a$ ) and crystallization temperature ( $T_c$ ) might be continued improved for high-density, low consumption PCM devices [10, 11].

Recently, in order to improve the activation energy and crystallization temperature, great efforts have been made, such as doping with matrix with N [12, 13], O [14], W [15], Se [16], Al [17], C [18], Si [19], Mg [20, 21], Cu [22] atoms, etc. In our previous work, it has been found that Er doped Sb [23], Er doped SnSb [24], Er doped GeSb [25] has a higher  $T_c$ , a bigger activation energy. In this paper, Er was chosen as the dopants and we systematically studied the phase change properties of Er doped SbSe thin films.

✉ Hua Zou  
zouhua@jsut.edu.cn

✉ Xiaoqin Zhu  
zxq@jsut.edu.cn

<sup>1</sup> School of Mathematics and Physics, Jiangsu University of Technology, Changzhou 213001, People’s Republic of China

<sup>2</sup> State Key Laboratory of Functional Materials for Informatics, Shanghai Institute of Micro-system and Information Technology, Chinese Academy of Sciences, Shanghai 200050, People’s Republic of China

## 2 Experimental details

The Erbium doped  $\text{Sb}_{70}\text{Se}_{30}$  thin films of  $\text{Er}_x(\text{Sb}_{70}\text{Se}_{30})_{1-x}$  ( $0 \leq x \leq 0.018$ ) were deposited on  $\text{SiO}_2/\text{Si}$  (100) wafers by co-sputtering of Er and  $\text{Sb}_{70}\text{Se}_{30}$  targets at room temperature using magnetron sputtering. The purity of  $\text{Sb}_{70}\text{Se}_{30}$  and Er targets was 99.999%. The base pressure in the deposition chamber was  $2 \times 10^{-4}$  Pa. Sputtering was performed under the Ar gas pressure of 0.3 Pa, the flow of 30 sccm, and the power of 30 W. The thin film thickness was set to 50 nm through controlling deposition time. To ensure the uniformity of deposition, the substrate holder was rotated at an autorotation speed of 20 rpm.

The amorphous to crystalline transition was investigated by in situ temperature-dependent resistance (R–T) measurement using a TP 95 temperature controller (Linkam Scientific Instruments Ltd, Surry, UK) under Ar atmosphere. The reflectivity of the films was measured in the range of 800–2500 nm by NIR spectrophotometer (7100CRT, XINMAO, China). The crystalline structures of the films were analyzed by X-ray diffraction (XRD). The speed of phase change was characterized by a picoseconds laser pumping probe system. The He–Ne laser with a wavelength of 632.8 nm was used as a probing laser. The laser irradiating was performed to films using a mode-locked neodymium-doped yttrium aluminum garnet laser operating at 532 nm wavelength with approximately 30 ps. The compositions of deposited films were determined by means of energy dispersive spectroscopy (EDS). In order to assess the chemical bonding states of Er doped  $\text{Sb}_{70}\text{Se}_{30}$  film, the X-ray photoelectron spectroscopy (XPS) was carried out.

## 3 Results and discussions

The R–T curves for Er doped  $\text{Sb}_{70}\text{Se}_{30}$  films as shown in Fig. 1a were measured with a heating rate of  $20^\circ\text{C}/\text{min}$ . As shown in the figure, the crystallization temperature ( $T_c$ ), which is identified by the derivative of resistance with respect to the temperature ( $dR/dT$ ), increases with increasing the Er doping content. Thus, it can be seen that the Er doping will promote the stability of phase change materials for PCM application. In addition, the resistance of amorphous and crystalline state of  $\text{Er}_{0.012}(\text{Sb}_{70}\text{Se}_{30})_{0.988}$  is about one order than the pure  $\text{Sb}_{70}\text{Se}_{30}$ . In general, the higher resistance of materials can facilitate heating under pulse current, revealing the lower power consumption of the PCM devices. Figure 1a also reveals that the  $\text{Sb}_{70}\text{Se}_{30}$  film would no longer possess phase change properties when the doping concentration up to 1.8%.

The diffuse reflectivity spectra of amorphous  $\text{Er}_x(\text{Sb}_{70}\text{Se}_{30})_{1-x}$  films were measured at room temperature in the wavelength ranging from 800 to 2500 nm. Generally, the conversion of reflectivity to absorbance data can be obtained by the Kubelka–Munk function [26]:

$$K/S = (1 - R)^2/2R \quad (1)$$

where R is the reflectivity, K is the absorption coefficient and S is the scattering coefficient. Then, the values of optical band gap energy ( $E_g$ ) were defined from the intercept on the energy axis with zero absorbance as shown in Fig. 1b. It is obvious that the  $E_g$  increases from the 1.41 to 1.68 eV with increasing the Er doping. In semiconductor materials, the increase of  $E_g$  would lead to the reduction in carriers and the decrease of carrier density, revealing increasing the resistance of the materials. Thus, this result and hypothesis point out that the Er dopants can change the  $E_g$  and then increase the resistance.

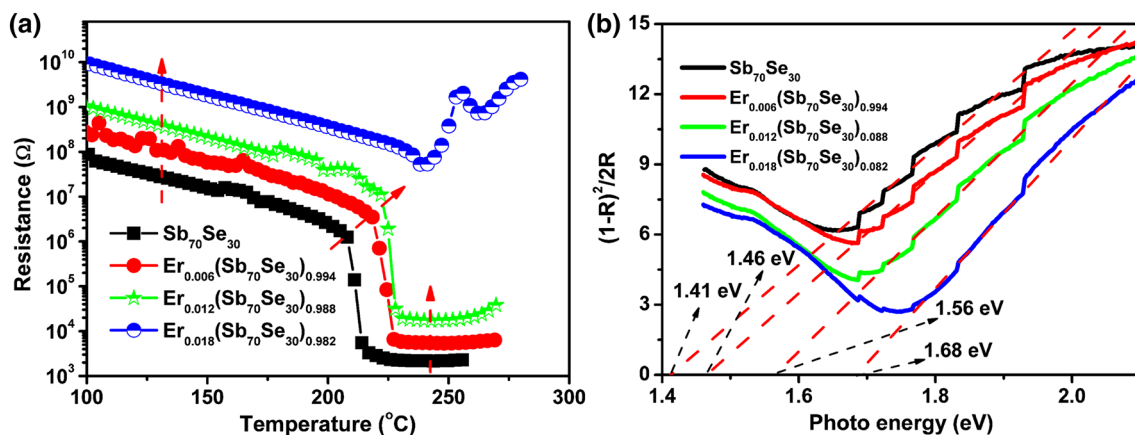


**Fig. 1** a The sheet resistance as a function of temperature. b The Kubelka–Munk function for pure  $\text{Sb}_{70}\text{Se}_{30}$  and Er doped  $\text{Sb}_{70}\text{Se}_{30}$  thin films

In general, the energy activation ( $E_a$ ) is used as the first indication of data stability [27]. The resistivity in situ measures at various heating rates ( $dT/dt$ ) and then the  $E_a$  can be calculated by the Kissinger’s equation [28]:

$$\ln[(dT/dt)/T_c^2] = C - (E_a/k_B T_c) \tag{2}$$

where  $C$  is a constant and  $k_B$  is the Boltzmann constant. From the Kissinger plots, Fig. 2a depicts that the  $E_a$  are about 3.97 eV ( $Sb_{70}Se_{30}$ ), 4.40 eV [ $Er_{0.006}(Sb_{70}Se_{30})_{0.994}$ ], and 4.66 eV [ $Er_{0.012}(Sb_{70}Se_{30})_{0.988}$ ]. This result shows that the Er doping would increase the  $E_a$ , meaning improvement of data stability. The increase of  $E_a$  may be ascribed to the complex bonding environment in the amorphous phase. The isothermal change in resistance as function of temperature is another key index to judge the data retention  $Er_x(Sb_{70}Se_{30})_{1-x}$  films. The failure time is defined as the time when the resistance reaches half of its initial magnitude. Then the plot of failure time versus  $1/k_B T$  can be described as the Arrhenius’ equation [29]:

$$t = \tau_0 \exp(E_a/k_B T) \tag{3}$$

where the  $t$ ,  $\tau_0$ , and  $T$  are the failure time, pre-exponential factor depending on the materials’ properties and absolute temperature, respectively. As shown in Fig. 2b, it is obviously that the 10-year retention temperature increases from 126 to 150 °C by increasing the Er dopants. To compete with NOR-Flash memory, the data retention of 10 year for PCM at temperature should be higher than 125 °C [30]. From this perspective, the  $Er_{0.012}(Sb_{70}Se_{30})_{0.988}$  thin films process data retention of 150 °C, meeting the application of high performance PCM devices. In addition, the  $E_a$  calculated by Eq. (3) also gives the same trend compared with the Kissinger’s equation.

Film surface roughness significantly influences the devices performances because the electric properties relate to the quality of electric-film interface. Figure 3 shows root-mean-square (RMS) of the  $Er_{0.012}(Sb_{70}Se_{30})_{0.988}$  is 0.30 nm (as-prepared) and 0.54 nm (annealing at 250 °C). The higher surface roughness of annealed sample is attributed to its crystallization. Compared with GST [31], Al doped  $Sn_2Se_3$  [32], and Er doped  $Ge_{10}Sb_{90}$  [25], the Er doped  $Sb_{70}Se_{30}$

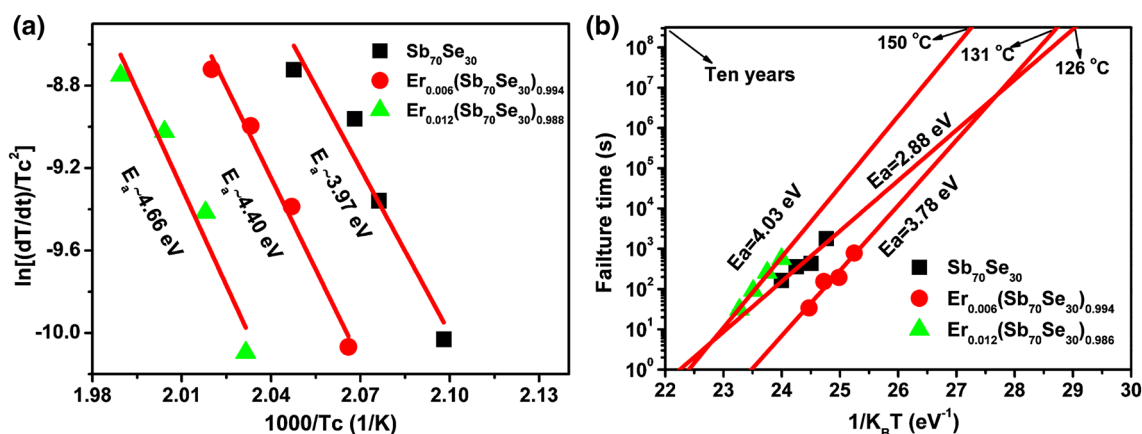
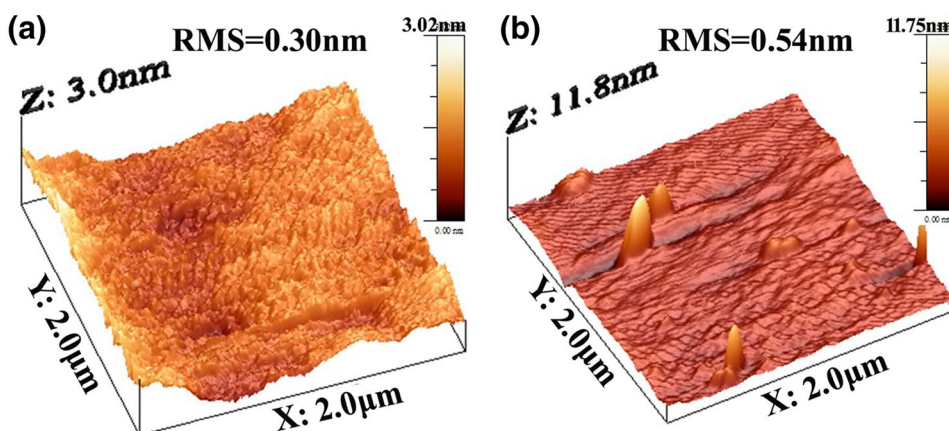


**Fig. 2** a Kissinger’s plot for estimated  $E_a$ . b Plots of failure times as a function of reciprocal temperature for pure  $Sb_{70}Se_{30}$  and Er doped  $Sb_{70}Se_{30}$  thin films

**Fig. 3** AFM image of a as-prepared and b annealed at 250 °C of  $Er_{0.012}(Sb_{70}Se_{30})_{0.988}$  thin film



films possess smaller surface roughness and grain sizes, which may attribute to higher crystallization temperature of  $\text{Sb}_{70}\text{Se}_{30}$  ( $\sim 210^\circ\text{C}$ ) than GST ( $\sim 160^\circ\text{C}$ ),  $\text{Sn}_2\text{Se}_3$  ( $200^\circ\text{C}$ ) and  $\text{Ge}_{10}\text{Sb}_{90}$  ( $189^\circ\text{C}$ ). This result indicates excellent electric behavior and low residual stress for PCM devices.

In general, Sb-rich alloys such as GaSb [33], GeSb [34], SnSb [35], have the advantage of very short crystallization times ( $<15\text{ ns}$ ). Thus, the phase change speed is one of the most parameters for the Er doped  $\text{Sb}_{70}\text{Se}_{30}$  alloys. Many works demonstrate that the phase change speed can be characterized by change in optical reflectivity. Figure 4

depicts the reflection spectrum measured by picoseconds laser pump–probe system. When a laser pulse with a fluence of  $0.85\text{ mJ/cm}^2$  is applied, the reflectivity of  $\text{Sb}_{70}\text{Se}_{30}$  decreases due to the crystalline-to-amorphous transition as shown in Fig. 4a. Correspondingly, the reflectivity spectra of  $\text{Er}_{0.012}(\text{Sb}_{70}\text{Se}_{30})_{0.988}$  films are also achieved with a fluence of  $1.30\text{ mJ/cm}^2$  in Fig. 4b. It is apparent that the Er doped  $\text{Sb}_{70}\text{Se}_{30}$  film possess much faster speed change speed. In this aspect, the Er doping can improve the speed change speed for PCM application.

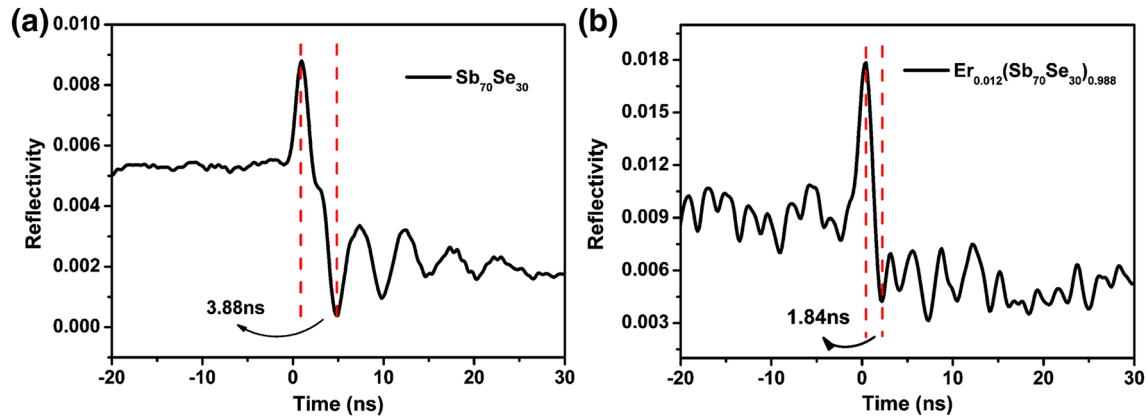
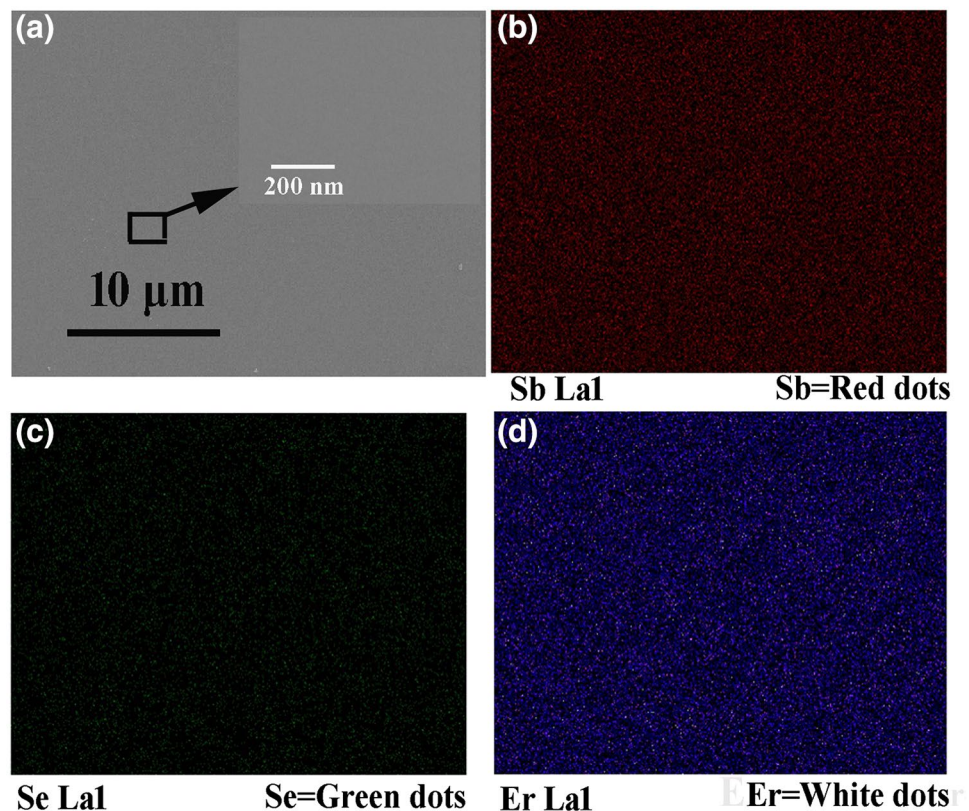


**Fig. 4** Reversible reflectivity evolution of **a**  $\text{Sb}_{70}\text{Se}_{30}$  and **b**  $\text{Er}_{0.012}(\text{Sb}_{70}\text{Se}_{30})_{0.988}$  thin films induced by two consecutive picoseconds laser pulses

**Fig. 5** The SEM and EDS result of the as-prepared  $\text{Er}_{0.012}(\text{Sb}_{70}\text{Se}_{30})_{0.988}$  thin films mapping: **a** SEM image and **b–d** corresponding images of EDS element distribution mapping



SEM–EDS element distribution mapping is a useful tool to identify chemical composition. Figure 5 shows the SEM–EDS result of the  $\text{Er}_{0.012}(\text{Sb}_{70}\text{Se}_{30})_{0.988}$  thin films. From Fig. 5a, it can be seen that no crystalline grains are observed, which is consistent with the AFM measurement. The corresponding EDS mapping images, as shown in Fig. 5b–d, have visible and well-dispersed spot distributions, which directly demonstrate the existence of Sb, Se, and Er elements. In addition, the results indicate that the Sb, Se and Er are distributed uniformly in the amorphous state.

Figure 6a shows the XRD patterns of pure  $\text{Sb}_{70}\text{Se}_{30}$  annealed isothermally at different temperature for 10 min. One board peak of sample annealed at 200 °C reveals that the pure  $\text{Sb}_{70}\text{Se}_{30}$  is amorphous even after annealed at 200 °C. When annealing temperature up to 230 °C, the hexagonal Sb phase emerges, which also confirm that the resistivity drop caused by the amorphous-to-crystalline phase transition. By increasing annealing temperature up to

260 °C, the stable phases for the  $\text{Sb}_{70}\text{Se}_{30}$  are the mixture of Sb and  $\text{Sb}_2\text{Se}_3$ . However, in the case of the Er doped  $\text{Sb}_{70}\text{Se}_{30}$  film, the distinct  $\text{Sb}_2\text{Se}_3$  peak was not observed even after annealed at 270 °C. This could imply that the Er doping inhibit the Sb–Sb and Sb–Se crystallization process with the crystallization mechanism of growth dominant, which may ascribe to the preliminarily formation of Er–Sb bond requiring higher  $E_a$ . Generally, only the Sb phase in Er doped  $\text{Sb}_{70}\text{Se}_{30}$  crystalline films is favorable since more Sb phase represents much faster phase change speed. Thus, the improvement of phase change speed can be assigned to the single Sb phase in Er doped  $\text{Sb}_{70}\text{Se}_{30}$  alloys.

In order to clarify the role of Er in the  $\text{Sb}_{70}\text{Se}_{30}$  alloys, we examined the Sb 3d and Se 3d XPS peaks for pure  $\text{Sb}_{70}\text{Se}_{30}$  (annealed at 260 °C for 10 min) and  $\text{Er}_{0.012}(\text{Sb}_{70}\text{Se}_{30})_{0.988}$  (annealed at 270 °C for 10 min). Figure 7a shows the peaks of Sb 3d slightly shift to a lower region after Er doping, which reveals the formation of the Er–Sb bond. In addition,

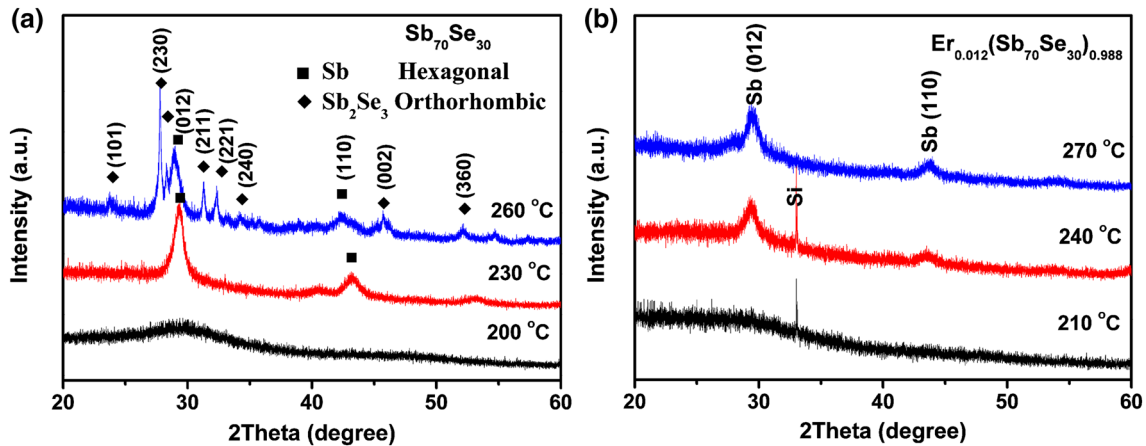


**Fig. 6** XRD patterns of **a** pure  $\text{Sb}_{70}\text{Se}_{30}$  and **b**  $\text{Er}_{0.012}(\text{Sb}_{70}\text{Se}_{30})_{0.988}$  thin films annealed at different temperature in Ar atmosphere for 10 min

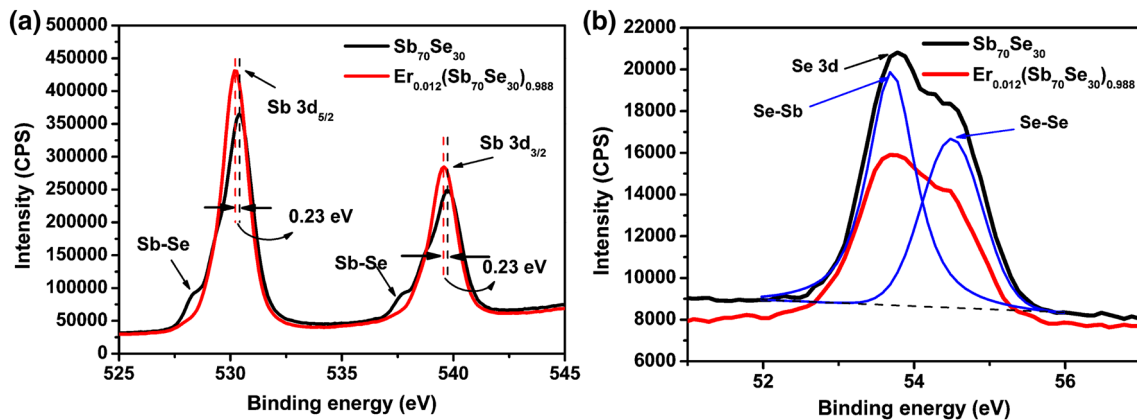


**Fig. 7** XPS spectra of **a** Sb 3d and **b** Se 3d of crystalline pure  $\text{Sb}_{70}\text{Se}_{30}$  thin film and  $\text{Er}_{0.012}(\text{Sb}_{70}\text{Se}_{30})_{0.988}$  thin film

the peaks at 528.1 and 537.5 eV only in pure  $\text{Sb}_{70}\text{Se}_{30}$  are assigned to orthorhombic  $\text{Sb}_2\text{Se}_3$  phase with the Sb–Se bond. This is consistent with the XRD measurement. The Se 3d peaks are shown in Fig. 7b. It reveals that the pure  $\text{Sb}_{70}\text{Se}_{30}$  and Er doped  $\text{Sb}_{70}\text{Se}_{30}$  thin films both have the Se–Sb and Se–Se bond. More importantly, it can be shown that Sb 3d peak intensity increase and Se 3d peak intensity decrease by Er doping. In general, increased bond induces higher relatively intensity in XPS spectra. Thus, this result reveals the increase of Sb–Sb bonding and decrease of Sb–Se bonding after the Er doping, which match the faster phase change speed by Er doping.

## 4 Conclusions

In summary, Er doped  $\text{Sb}_{70}\text{Se}_{30}$  thin films were prepared by magnetron sputtering technique. The various electrical and structural properties for PCM application are examined as a function of the Er doping content. When Er doped into  $\text{Sb}_{70}\text{Se}_{30}$  film, the  $T_c$ ,  $E_a$ ,  $E_g$ , resistance and 10-year data retention temperature increase significantly, which indicate the improvement of the thermal stability and power consumption for PCM application. Furthermore, The XPD and XPS measurement prove that Er doping inhibits the formation of Sb–Se bond, which give rise to much faster of phase change speed. In addition, the Er doped films have well-uniform Er dopants, low surface roughness and small grain sizes, indicating excellent electric behavior for PCM devices.

**Acknowledgements** The work was supported by Natural Science Foundation of Jiangsu Province (No. BK20151172), Changzhou Sci&Tech Program (Nos. CJ20159049, CJ20160028), and sponsored by Qing Lan Project.

### Compliance with ethical standards

**Conflict of interest** The authors declare that they have no conflicts of interest to this work.

## References

- M. Wuttig, Phase-change materials: towards a universal memory? *Nat. Mater.* **4**, 265–266 (2005)
- X. Zhou, J. Kalikka, X. Ji, L. Wu, Z. Song, R.E. Simpson, Phase-change memory materials by design: a strain engineering approach. *Adv. Mater.* **28**, 3007–3016 (2016)
- S. Raoux, D. Ielmini, Phase change materials and their application to nonvolatile memories. *Chem. Rev.* **110**, 240–267 (2009)
- S. Hudgens, B. Johnson, Overview of phase-change chalcogenide nonvolatile memory technology. *MRS Bull.* **29**, 829–832 (2004)
- Y. Lu, M. Stegmaier, P. Nukala, M.A. Giambra, S. Ferrari, A. Busacca, W.H. Pernice, R. Agarwal, Mixed-mode operation of hybrid phase-change nanophotonic circuits. *Nano Lett.* **17**, 150–155 (2016)
- D. Lencer, M. Salinga, B. Grabowski, T. Hickel, J. Neugebauer, M. Wuttig, A map for phase-change materials. *Nat. Mater.* **7**, 972–977 (2008)
- Y. Lu, S. Song, Z. Song, L. Wu, A. He, Y. Gong, F. Rao, B. Liu, Superlattice-like electrode for low-power phase-change random access memory. *Appl. Phys. Lett.* **101**, 113104 (2012)
- Y. Lu, S. Song, X. Shen, Z. Song, G. Wang, S. Dai, Study on phase change properties of binary GaSb doped Sb–Se film. *Thin Solid Films* **589**, 215–220 (2015)
- Y. Sung-Min, L. Nam-Yeal, R. Sang-Ouk, C. Kyu-Jeong, Y.S. Park, L. Seung-Yun, Y. Byoung-Gon, K. Myung-Jin, C. Se-Young, M. Wuttig, Sb-Se-based phase-change memory device with lower power and higher speed operations. *IEEE Electron. Dev. Lett.* **27**, 445–447 (2006)
- M.J. Kang, T.J. Park, D. Wamwangi, K. Wang, C. Steimer, S.Y. Choi, M. Wuttig, Electrical properties and crystallization behavior of  $\text{Sb}_x\text{Se}_{100-x}$  thin films. *Microsyst. Technol.* **13**, 153–159 (2007)
- Y. Lu, S. Song, X. Shen, L. Wu, Z. Song, B. Liu, S. Dai, Q. Nie, Investigation of Ga8Sb34Se58 material for low-power phase change memory. *ECS Solid State Lett.* **2**, P94-P96 (2013)
- L. Cheng, L. Wu, Z. Song, F. Rao, C. Peng, D. Yao, B. Liu, L. Xu, Effects of germanium and nitrogen incorporation on crystallization of N-doped  $\text{Ge}_2 + x\text{Sb}_2\text{Te}_5$  ( $x = 0,1$ ) thin films for phase-change memory. *J. Appl. Phys.* **113**, 044514 (2013)
- S.Y. Lee, H.K. Kim, J.H. Kim, J.S. Roh, D.J. Choi, Phase transition characteristics and electrical properties of nitrogen-doped GeSb thin films for PRAM applications. *J. Mater. Sci.* **44**, 4354–4359 (2009)
- Y. Hu, M. Sun, S. Song, Z. Song, J. Zhai, Oxygen-doped  $\text{Sb}_4\text{Te}$  phase change films for high-temperature data retention and low-power application. *J. Alloys Compd.* **551**, 551–555 (2013)
- N. Ciocchini, E. Palumbo, M. Borghi, P. Zuliani, R. Annunziata, D. Ielmini, Modeling resistance instabilities of set and reset states in phase change memory with Ge-Rich GeSbTe. *IEEE Trans. Electron. Dev.* (2014). doi:10.1109/TED.2014.2313889
- E.M. Vinod, A.K. Singh, R. Ganesan, K.S. Sangunni, Effect of selenium addition on the GeTe phase change memory alloys. *J. Alloys Compd.* **537**, 127–132 (2012)
- G. Wang, X. Shen, Q. Nie, R. Wang, L. Wu, Y. Lv, F. Chen, J. Fu, S. Dai, J. Li, Improved thermal and electrical properties of Al-doped  $\text{Ge}_2\text{Sb}_2\text{Te}_5$  films for phase-change random access memory. *J. Phys. D* **45**, 375302 (2012)
- X. Zhou, L. Wu, Z. Song, F. Rao, M. Zhu, C. Peng, D. Yao, S. Song, B. Liu, S. Feng, Carbon-doped  $\text{Ge}_2\text{Sb}_2\text{Te}_5$  phase change material: a candidate for high-density phase change memory application. *Appl. Phys. Lett.* **101**, 202 (2012)
- L. Tong, L. Xu, Y. Jiang, F. Yang, L. Geng, J. Xu, W. Su, Z. Ma, K. Chen, Improved phase-change characteristics of Si doped GeSbTe thin films used for phase change memory. *J. Non-Cryst. Solids* **358**, 2402–2404 (2012)
- J. Fu, X. Shen, Q. Nie, G. Wang, L. Wu, S. Dai, T. Xu, R.P. Wang, Crystallization characteristics of Mg-doped  $\text{Ge}_2\text{Sb}_2\text{Te}_5$  films for phase change memory applications. *Appl. Surf. Sci.* **264**, 269–272 (2013)
- X. Shen, J. Li, G. Wang, Z. Wang, Y. Lu, S. Dai, Fast crystallization of Mg-doped  $\text{Sb}_4\text{Te}$  for phase change memory. *Vacuum* **112**, 33–37 (2015)
- S. Raoux, M. Salinga, J.L. Jordan-Sweet, A. Kellock, Effect of Al and Cu doping on the crystallization properties of the phase change materials SbTe and GeSb. *J. Appl. Phys.* **101**, 044909 (2007)
- H. Zou, X. Zhu, Y. Hu, Y. Sui, W. Wu, J. Xue, L. Zheng, Z. Song, Improvement of the thermal stability of Sb thin film through erbium doping. *CrystEngComm* **18**, 6365–6369 (2016)
- H. Zou, X. Zhu, Y. Hu, Y. Sui, Y. Sun, J. Zhang, L. Zheng, Z. Song, Simultaneous thermal stability and phase change speed

- improvement of Sn<sub>15</sub>Sb<sub>85</sub> thin film through erbium doping. *J. Appl. Phys.* **120**, 245303 (2016)
25. H. Zou, Y. Hu, X. Zhu, Y. Sun, L. Zheng, Y. Sui, S. Wu, Z. Song, Improvement in reliability and power consumption based on Ge<sub>10</sub>Sb<sub>90</sub> films through erbium doping. *J. Mater. Sci.* **52**, 5216–5222 (2017)
26. S. Tandon, J. Gupta, Measurement of forbidden energy gap of semiconductors by diffuse reflectance technique. *Physica Status Solidi B* **38**, 363–367 (1970)
27. M.J. Kang, S.Y. Choi, D. Wamwangi, K. Wang, C. Steimer, M. Wuttig, M.J. Kang, et al., Structural transformation of Sb<sub>x</sub>Se<sub>100-x</sub> thin films for phase change nonvolatile memory applications. *J. Appl. Phys.* **98**, 014904–014906 (2005)
28. F. Liu, X. Liu, Q. Wang, Examination of Kissinger's equation for solid-state transformation. *J. Alloys Compd.* **473**, 152–156 (2009)
29. K.J. Laidler, The development of the Arrhenius equation. *J. Chem. Educ.* **61**, 494 (1984)
30. T. Morikawa, K. Kurotsuchi, Y. Fujisaki, Y. Matsui, N. Takaura, Characterization of In<sub>20</sub>Ge<sub>15</sub>Sb<sub>10</sub>Te<sub>55</sub> phase change material for phase change memory with low power operation and good data retention. *Jpn. J. Appl. Phys.* **51**, 031201 (2012)
31. S. Song, Z. Song, L. Wu, B. Liu, S. Feng, Stress reduction and performance improvement of phase change memory cell by using Ge<sub>2</sub>Sb<sub>2</sub>Te<sub>5</sub>-TaOx composite films. *J. Appl. Phys.* **109**, 034503 (2011)
32. Y. Hu, S. Li, T. Lai, S. Song, Z. Song, J. Zhai, Fast crystallization and low power of Al-doped Sn<sub>2</sub>Se<sub>3</sub> thin films for phase change memory applications. *J. Alloys Compd.* **581**, 515–518 (2013)
33. M. Putero, M.-V. Coulet, T. Ouled-Khachroum, C. Muller, C. Baehitz, S. Raoux, Unusual crystallization behavior in Ga-Sb phase change alloys. *APL Mater.* **1**, 062101 (2013)
34. C. Cabral Jr., L. Krusin-Elbaum, J. Bruley, S. Raoux, V. Deline, A. Madan, T. Pinto, Direct evidence for abrupt postcrystallization germanium precipitation in thin phase-change films of Sb–15 at.% Ge. *Appl. Phys. Lett.* **93**, 071906 (2008)
35. F. Rao, Z.T. Song, K. Ren, X.L. Li, L.C. Wu, W. Xi, B. Liu, Sn<sub>12</sub>Sb<sub>88</sub> material for phase change memory. *Appl. Phys. Lett.* **95**, 032105 (2009)